

Topographical site amplifications investigation by combining numerical and field experiments : the case of Rognes, south east France



N. Glinsky

IFSTTAR/CETE Méditerranée, Nice and INRIA Sophia Antipolis Méditerranée, France

E. Bertrand

CETE Méditerranée, Nice, France

SUMMARY:

Seismological recordings allow examining local seismicity and teleseismic events in various sites. From these data, we produce site transfer functions proving that each site has its own response. Numerical simulation is an interesting tool to understand and try reproducing these phenomena. In a previous work, we have used a discontinuous Galerkin finite element method to study the amplification, the concerned frequencies and their distribution along a realistic 2D profile of the Rognes area (France) for series of vertical plane waves of various frequencies. The comparison of numerical results with real measurements confirmed the site effect and the influence of the topography but also the importance of the model in depth-geometry. The objective, here, is to investigate the combined effects of steepness, heterogeneity and angle of incidence on the surface response, considering a simplified topography and the realistic 2D profile of the Rognes area.

Keywords: Site effect, numerical simulation, discontinuous Galerkin, plane wave, Rognes.

1. INTRODUCTION

Many experimental records have been performed during the last 20 years by the CETE Méditerranée Seismic Risk team. This allowed recording local seismicity and teleseismic events in different sites, in France and elsewhere, and in many geological configurations: sedimentary basins, deep alluvial sites, topographic profiles and flat rock sites. Their processing produces site transfer functions that prove that each site has its own response (Bertrand *et al.*, 2011, Duval, 2007). Numerical simulation of wave propagation on realistic topographies is an interesting tool which helps understanding the observed ground motion amplification and their variability. Various numerical methods have been developed for computational seismology within the last few decades; we use the discontinuous Galerkin finite element (DG) method (Delcourte *et al.*, 2009).

The Provence earthquake, which occurred in 1909 in the south of France, is the most significant earthquake of the 20th century (estimated magnitude 6) in France. It particularly caused severe damage in the small village of Rognes, built on the Foussa hill, probably due to site effects. To highlight this, the CETE Méditerranée Seismic Risk team conducted a field operation, between 2007 and 2009, achieving continuous recordings on nine selected sites (see Fig. 1.1 for some of them). This campaign allowed recording and analysing more than 70 earthquakes (10 local and 60 teleseismic events). Three processing have been conducted from these data: H/V ratio on ambient vibration, H/V ratio on earthquake and site/reference standard spectral ratios (SSR) on earthquakes (Duval *et al.*, 2009).

In a previous work (Glinsky and Bertrand, 2011), the DG method has been applied to a two-dimensional south-north cross-section of the Foussa hill (as shown on Fig. 1.1, blue line) in order to reproduce numerically the results obtained by Duval *et al.* (2009) and study the amplification, the concerned frequencies and their distribution along this realistic two-dimensional topography. For this, we examined the seismic response of this profile to series of vertical plane waves of various frequencies by computing the amplification ratios at some virtual stations located at its surface.

Several homogeneous and heterogeneous configurations have been considered and the first conclusion is that the results are very dependent on the medium characteristics especially the model in depth-geometry and the model velocity contrast. These numerical solutions have been compared to real measurements data and a very good accordance has been obtained for a heterogeneous model constituted by two different media including a lower velocity medium for the entire hill.

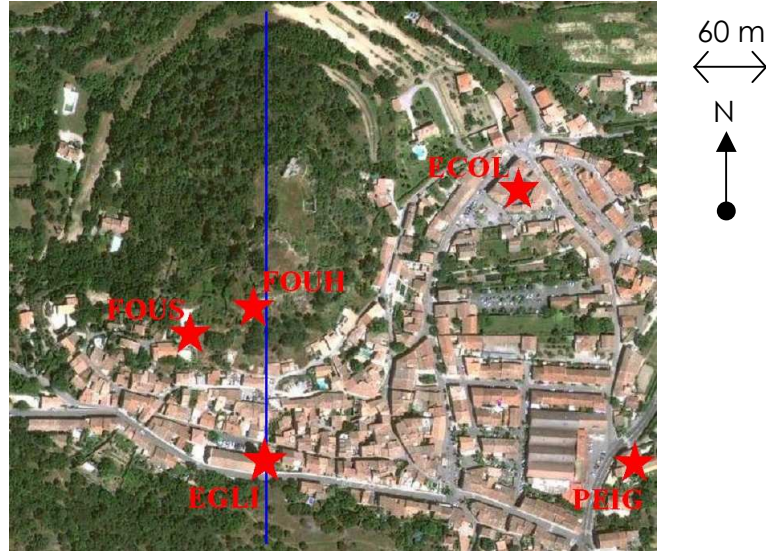


Figure 1.1. Aerial photography of the studied zone and location of some stations. The blue line corresponds to the south-north profile used in the modeling.

In this paper, we try to explain these phenomena and, first, consider a simplified profile, as done by Gaffet and Bouchon (1989), and investigate the influence of this topography on surface motion. We focus on the effect of several parameters, such as the steepness of the hill, the model in depth-geometry and the angle of incidence. In a second part, we improve the previous study (Glinsky and Bertrand, 2011), by considering the same 2D realistic topography of the Rognes area and propose an extension to non-vertical incident planes waves.

2. EQUATIONS AND NUMERICAL METHOD

We consider a two-dimensional isotropic, linearly elastic medium and solve the first-order velocity-stress system in time-domain:

$$\begin{cases} \rho \partial_t \bar{v} = \nabla \cdot \sigma, \\ \partial_t \sigma = \lambda (\nabla \cdot \bar{v}) Id + \mu (\nabla \bar{v} + (\nabla \bar{v})^t), \\ \sigma \bar{n} = \bar{0} \text{ on free surface} \end{cases} \quad (2.1)$$

where the unknowns are the velocity vector \bar{v} and the stress tensor σ . ρ , λ and μ are respectively the density of the medium and the Lamé coefficients. Id is the identity matrix and ∂_t stands for $\partial/\partial t$. This system is approximated by a discontinuous Galerkin finite element method, detailed in Delcourte *et al.* (2009), and summarized here only in few keywords. The physical domain is discretized using a finite element type mesh in triangles. The interpolation is based on Lagrange polynomials of degree 2. These basis functions are defined locally on each triangle which results in numerical fluxes at the interfaces between triangles. These fluxes are estimated using a centered scheme and, for time integration, we apply a second-order leap-frog scheme. On boundaries, except for the topography where a free surface condition is applied, we consider an upwind scheme, which allows setting the

values of the incident plane wave, whatever its angle of incidence.

3. APPLICATION TO A SIMPLIFIED HILL TOPOGRAPHY

First of all, the numerical method has been applied to the study of the effect of simplified hill topography on surface motion. This study has several objectives: 1) validate the method for vertically incident SV plane waves and a homogeneous medium, 2) study the influence of the model in depth-geometry by considering a heterogeneous medium, and 3) investigate the effect of the angle of incidence on the surface motion by extending this study to non vertical incident plane waves.

3.1. Validation of the method – Influence of the hill steepness

The validation of the method is done by reproducing the study proposed by Gaffet and Bouchon (1989) who examine the response of a ridge-shaped topography and the effect of the surface steepness on the diffracted wave field. This test case has also been considered by Komatisch (1997) for the validation of the spectral finite element solver Specfem and, more recently, by De Martin and Kobayashi (2010), using the spectral finite element program Efispec2D. For this, we consider a simplified hill topography which surface is given by

$$s(x) = h(1 - a) \exp(-3a), \quad a = (x/l)^2 \quad (3.1)$$

where $h=500$ m is the height of the hill and l its half width, the steepness of the hill being modified via the parameter h/l . The medium is homogeneous and has the characteristics of the medium M1 given in table 3.1. The source excitation is a vertically incident plane SV wave with a Ricker wavelet time dependence of central frequency $f_c=2.0$ Hz. This corresponds to a characteristic dimensionless period $\eta = h/(V_s t_p)=1$, where t_p is the period of the pulse. Solutions are recorded at 197 surface receivers, uniformly distributed in the x interval $[-4890; 4890]$ and five different topographies of shape ratios h/l equal to 0.2, 0.375, 0.5, 0.6 and 0.75 have been considered, as presented in Fig. 3.1.

Table 3.1. Characteristics of the different media.

	ρ (kg/m^3)	V_p (m/s)	V_s (m/s)
M1	2000	1870	1000
M2	1500	935	500

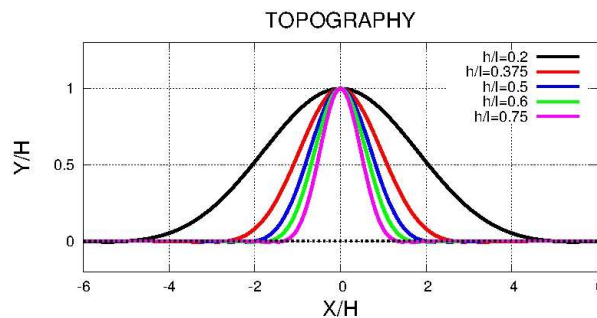


Figure 3.1. Simplified topography for different values of h/l .

For each value of h/l , we calculate the amplitude ratio as the ratio between the maximum of v_x recorded at the top of the hill (in $x=0$) and twice the maximum of the same component of the incident wave. We compare our values to the results of the discrete wavenumber-boundary integral equation method and the spectral finite element solvers. The different values of the amplitude ratio are listed in the table 3.2. We notice that the amplification is maximum for values of h/l equal to 0.375 and 0.5 and that our results are in perfect accordance with those of both spectral finite element

methods. Gaffet and Bouchon obtain higher values; Komatitsch attributes these differences to the high sensitivity of the amplitude at the top of the hill to constructive and destructive interferences. This constitutes a validation of our numerical method and the plane wave implementation.

Table 3.2. Amplitude ratio for different numerical methods

	Gaffet-Bouchon	Komatitsch	De Martin-Kobayashi	DG-fem
$h/l=0.2$			1.0	1.0
$h/l=0.375$	2.7	2.2	2.2	2.1
$h/l=0.5$	3.1	2.1	2.1	2.1
$h/l=0.6$			1.4	1.3
$h/l=0.75$	2.4	0.8	0.6	0.7

We plot, in Fig 3.2 and 3.3 (first line of figures, blue line), the distribution of amplification ratios at all surface receivers for h/l equal to 0.2, 0.375, 0.5 and 0.75. Here, the ratio is calculated by respect to the maximum values of the velocity norm (and not v_x), which allows including both components of the velocity and is more appropriate to non-vertical incident waves. We observe a clear amplification, mainly at the top of the hill, for values of h/l equal to 0.375 and 0.5, confirming the values given in table 3.2. Amplification is maximum at the top of the hill, except for $h/l=0.75$.

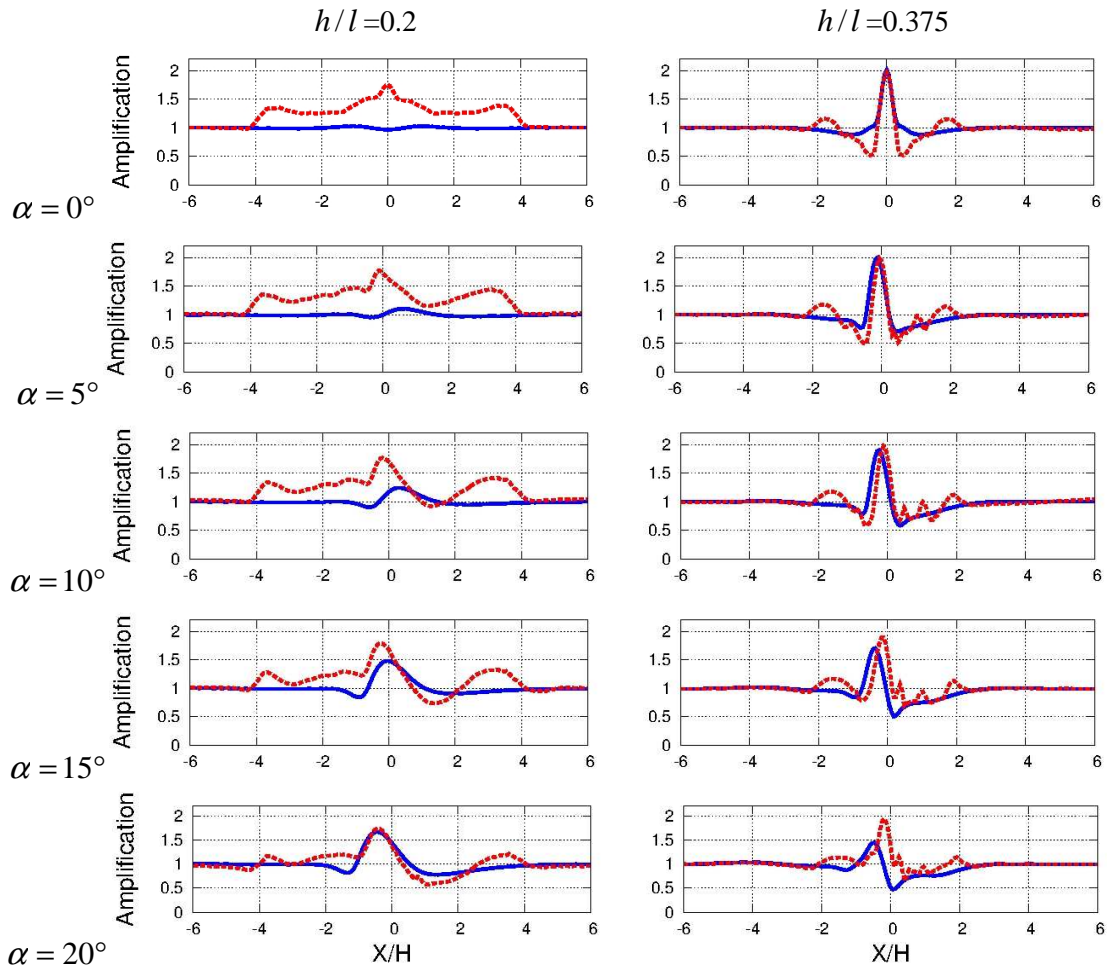


Figure 3.2. Amplification ratio at the surface of the simplified topography for $h/l=0.2$ (left column) and $h/l=0.375$ (right column). Blue lines correspond to the homogeneous medium and dashed red lines to the heterogeneous case. Each line of figures is associated to the incidence angle of the plane wave.

3.2. Heterogeneous hill model – Influence of the model in depth-geometry

To improve this study, we consider the case of a heterogeneous model and suppose that the entire hill is constituted by a lower velocity medium, referred as M2 in table 3.1, making reference to the results obtained for a 2D profile of the Rognes area (Glinsky and Bertrand (2011)). Then, as depicted in Fig. 3.1, above the dashed black line, the medium is M2 and, under this line, the medium is homogeneous and has the characteristics of M1. We reproduce the same study as previously, keeping the simplified hill profile and the incident vertical S-plane wave and present, in Fig. 3.2 and 3.3 (first line of figures, red dashed line), the results for the amplitude ratios at the surface for different values of h/l . Comparing the results of both homogeneous and heterogeneous cases, we notice very different behaviors according to the value of h/l . For $h/l=0.2$ which corresponds to a hill of small steepness, the heterogeneity results in a clear amplification, on the entire hill and not only at its top, while no amplification is recorded in the homogeneous case. At moderate steepness, for $h/l=0.375$, amplification is the same in both cases close to the top, but desamplification appears at the sides of the hill in the heterogeneous case. For higher values of h/l , the surface amplification profiles become more complex. For $h/l=0.5$, we note a clear decrease of amplification at the top of the hill for the heterogeneous case, whereas, for $h/l=0.75$, amplification occurs on both sides of the top and is lightly higher in the heterogeneous case.

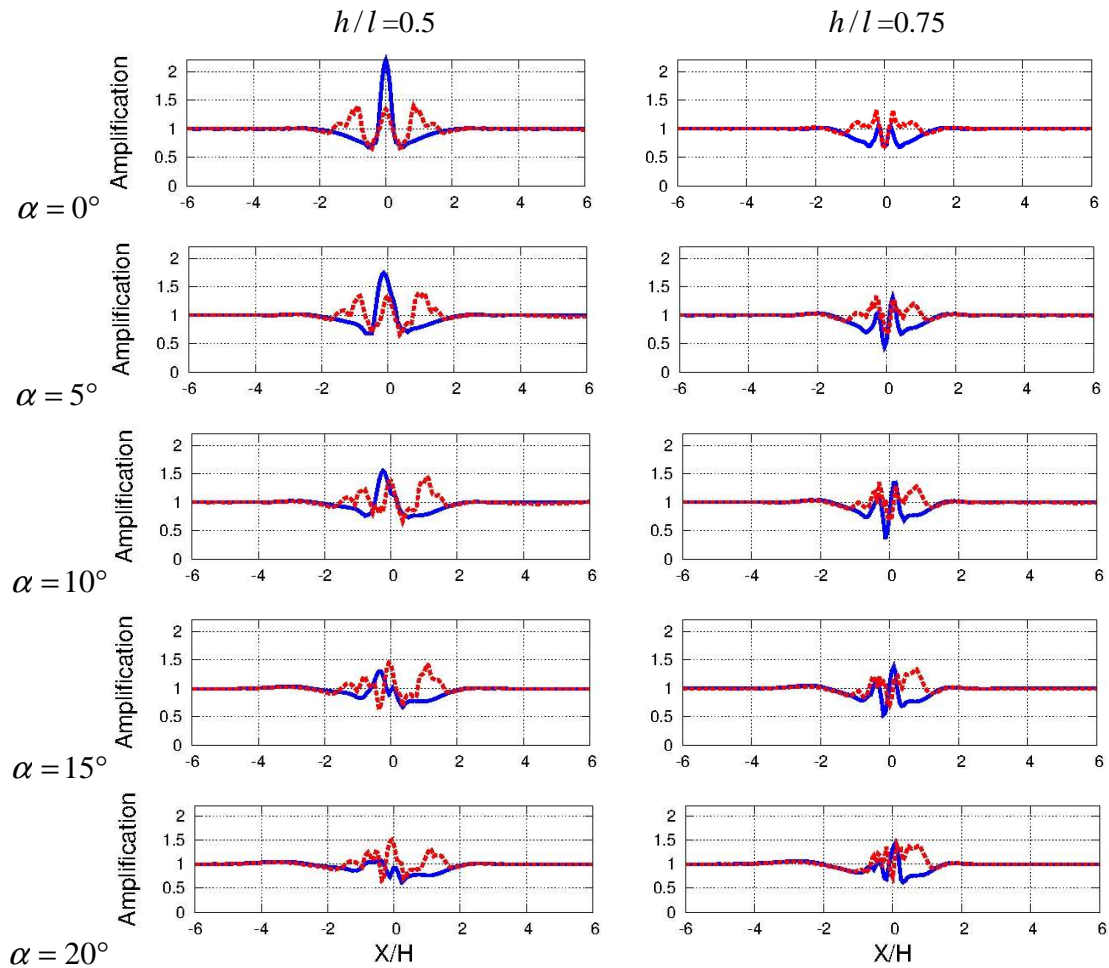


Figure 3.3. Amplification ratio at the surface of the simplified topography for $h/l=0.5$ (left column) and $h/l=0.75$ (right column). Blue lines correspond to the homogeneous medium and dashed red lines to the heterogeneous case. Each line of figures is associated to the incidence angle of the plane wave.

3.1. Non vertical incident plane waves – Influence of the angle of incidence

Finally, we conclude this study by investigating the effect of the angle of incidence on the surface motion. For this, we consider, as previously, homogeneous and heterogeneous models and different

values for the parameter h/l . Series of incident SV plane waves are deduced from the vertical case by a rotation of angle α . The topography being symmetrical, we consider only positive values of α taken in the set $\{5^\circ, 10^\circ, 15^\circ, 20^\circ\}$. We present amplification ratios obtained at the various surface receivers in Fig. 3.2 and 3.3, for the different values of the angle of incidence. As previously, the blue line is concerned with the homogeneous medium and the dashed red line with the heterogeneous case. For $h/l=0.2$ and homogeneous case, Fig. 3.2, the maximum of amplification increases with the angle of incidence and the location of this maximum moves from the right side to the left side of the hill. The heterogeneity strongly increases the amplification. Its maximum value remains quite independent on α and located very close to the top. For $h/l=0.375$ and $h/l=0.5$, in the homogeneous case, as α increases, the maximum of amplification reduces and moves to the left part of the hill. In the heterogeneous case, the profiles become more complex but the maximum remains quite constant and located close to the top of the hill. Finally, for highest steepness, $h/l=0.75$, the results are not very dependent on the angle of incidence or on the type of medium. In all cases, amplification is moderate and maximum in both sides of the hill.

4. APPLICATION TO A REALISTIC PROFILE OF THE ROGNES AREA

For this second part, a 2D realistic profile has been extracted from the topography of the Rognes area (blue line, Fig. 1.1), as done in Glinsky and Bertrand (2011). The two-dimensional domain is 10km wide and 6km deep. The upper boundary is the topography (as shown in Fig. 4.1), on which a free surface condition is applied. The mesh is composed of 512 000 triangles whose smallest edge is about 12.5 m. Seven sensors are virtually placed at different locations of the hill surface (as depicted in Fig. 4.1). These sensors are located similarly to the sites of the real data set (for instance, station 5 and the “FOUH” site at the top of the hill). The medium is heterogeneous and composed of M2 between the surface and the red line (as described in Fig. 4.1) and the medium M1 elsewhere. The characteristics of the media M1 and M2 are the same as for the simplified hill of the previous section and can be found in table 3.1. This model in depth-geometry has been chosen, following the results previously obtained in Glinsky and Bertrand (2011) for series of vertically incident SV plane waves of central frequencies between 0.2Hz and 10.0Hz, because solutions were in best accordance with real measurements data.

To link this study to the previous section, if the height of the major hill of the topography is about 70m and its half width approximately 300m, the ratio h/l is about 0.2 which can be compared to the first case of simplified topography. This value of the steepness is the most sensitive to the heterogeneity and to the angle of incidence.

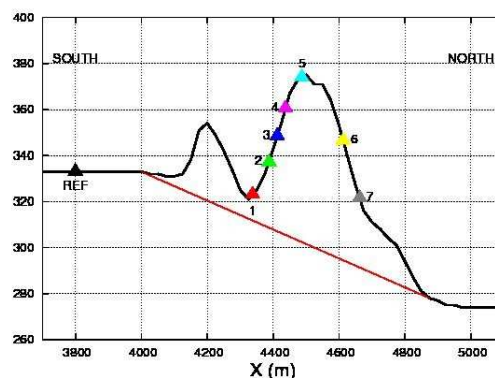


Figure 4.1. South-north 2D profile of the Rognes area and virtual sensors location (right picture). Low velocity medium M2 between surface and red line, medium M1 elsewhere.

We proceed to the propagation of series of vertical SV plane waves by solving Eqn. 2.1. In order to cover the frequency range $[0.2;10]$, we study two series of incident Ricker wavelets of central frequencies $f_c=2.0\text{Hz}$ and $f_c=5.0\text{Hz}$. Various angles of incidence α have been considered, taken in

the set $\{-20^\circ, -15^\circ, -10^\circ, -5^\circ, 0^\circ, 5^\circ, 10^\circ, 15^\circ, 20^\circ\}$. For each simulation (i.e. for each incident wave of central frequency f_c and for each angle α) and at each station, we obtain the velocity time history of both velocity components. Then, we apply the following procedure : 1) we compute the spectrum of both velocity components for each station as well as the reference solution, which is here twice the incident velocity. Note that for $\alpha=0^\circ$, this is only done for the horizontal component of the velocity. 2) we calculate the amplification ratios (station over reference) in an interval centered on f_c . 3) we construct the seismic response curve by gathering parts provided by results of both central frequencies.

We present, in Fig. 4.2, the seismic response derived from near earthquakes recordings at three particular sites (as presented on Fig. 1.1, Duval *et al.*, 2009). These sites can be compared to virtual stations of the 2D profile: station 4 to FOUS, station 5 to FOUH (at the top of the hill) and station 7 to ECOL. We observe that amplification is obtained at about 2.0Hz and 3.0Hz for stations FOUS, 2.0Hz and 4.0Hz for FOUH and approximatively at 5.0Hz for ECOL.

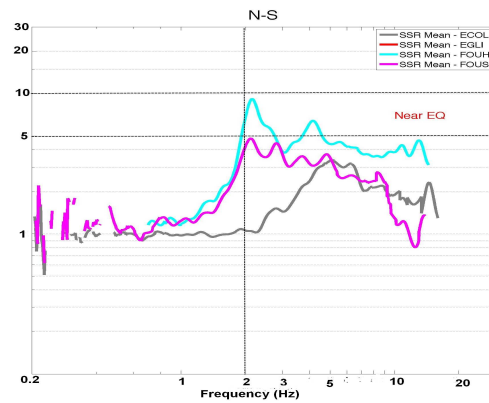


Figure 4.2. Seismic response at three stations from real measurements for near earthquakes.

The results of the numerical simulations corresponding to stations 4,5 and 7, for both velocity components and for all types of incidence are presented in Fig. 4.3. We choose to focus on these three particular stations and do not detail results obtained at other sensors, for a better comparison with the real data. Note that the medium is supposed linearly elastic which explains the differences at high frequencies.

From the observation of the results for the x-component of the velocity (left column of figures), we first notice that, for frequencies in $[0.2;2.5]$, the amplification curves are very similar whatever the angle of incidence. At stations 4 and 5, amplification is obtained at 2.0Hz which corresponds to the fundamental frequency of real measurements data. At station 7, it is clear that no amplification is measured between 0.2Hz and 2.0Hz as for real data. Amplification is maximum at 3.0Hz or 4.0Hz but results are not exactly the same for all values of α and amplification occurs for frequencies lower than for measurements data.

When examining the results for the vertical component of the velocity (right column of figures), we remark that these solutions are very dependent on the angle of incidence. At stations 4 and 5, amplification is obtained for higher frequencies, which seem to correspond to the second amplification of real data. Once more, results for station 7 do not correspond to measurements data. We can conclude that numerical results are similar to measurements data for stations 4 and 5 but not for station 7 which is located at the right side of the hill. The values of amplification are smaller for numerical simulations; this is perhaps due to the medium contrast between M1 and M2 (as studied in Glinsky and Bertrand, 2009) and also to the fact that both components are contained in amplification ratios of measurements data.

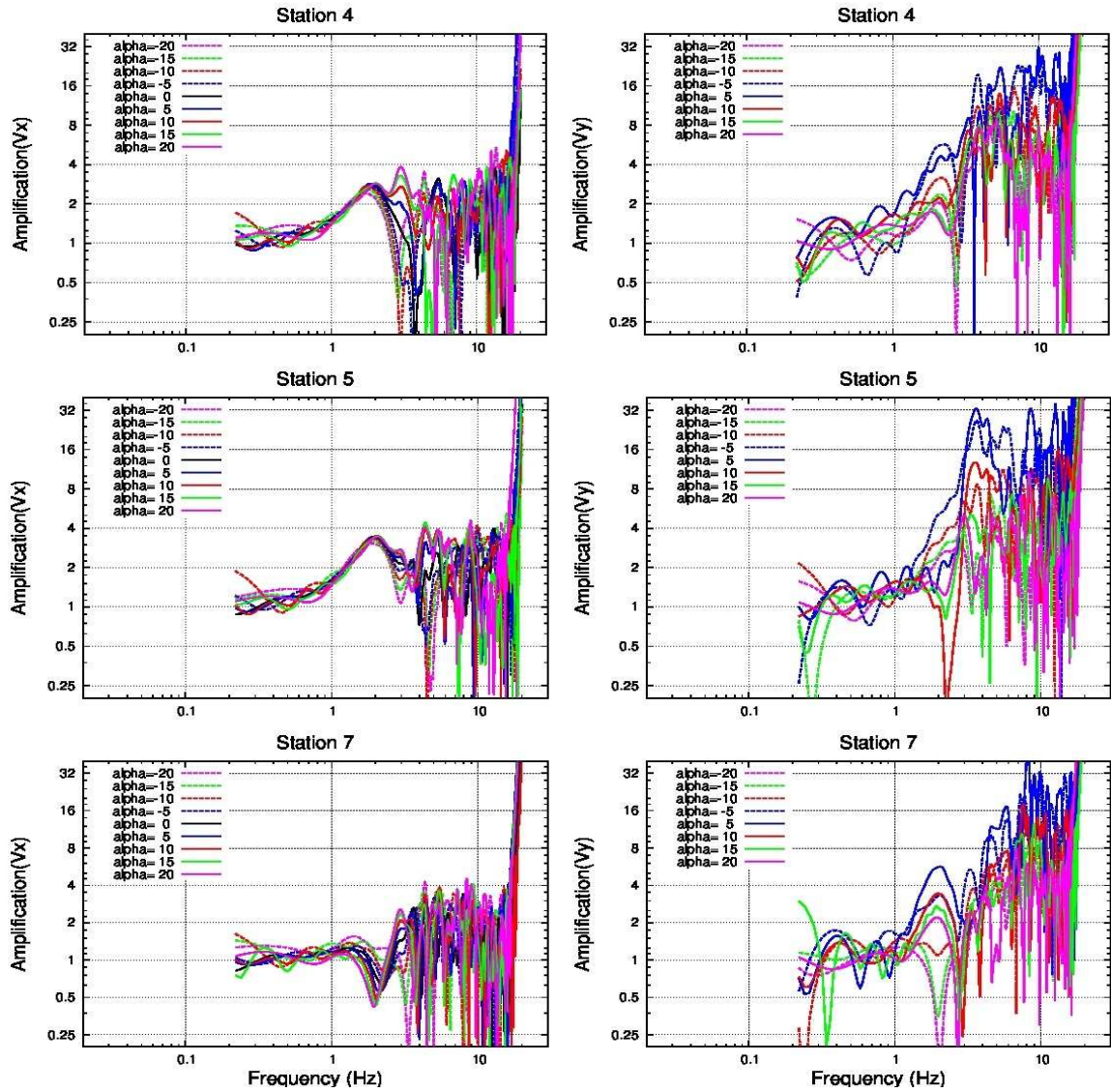


Figure 4.3. Seismic response at three virtual stations (station 4, first line of pictures, station 5, second line and station 7, last line of pictures). Amplification on v_x (left column) and v_y (right column) for different angles of incidence.

5. CONCLUSION

We present a study of topographical effects using numerical simulations by a discontinuous Galerkin finite element method. This method allows an accurate approximation of the topography via the use of triangular meshes and an easy inclusion of heterogeneities. A particular treatment at the boundaries allows non-vertical incident plane waves. This method has been applied to two types of investigations. First, we have studied the combined effects of steepness, heterogeneity and angle of incidence on the surface response, considering a simplified topography as proposed by Gaffet and Bouchon (1989). This test case allowed validating the numerical method and the plane wave implementation by comparison of our results to other numerical methods, for an homogeneous medium and a vertically incident SV plane wave. In a second step, we have studied the influence of heterogeneity by including a low velocity medium in the entire hill. This inclusion modifies the amplification at the surface, especially for small values of the steepness for which no amplification occur in the homogeneous case. Finally, series of non-vertical incident plane waves have been propagated and, once more, the small steepness case hill is the more sensitive to the angle of incidence.

A second application concerns a 2D realistic profile of the Rognes area. We have considered a heterogeneous model, following the conclusions of a previous study (Glinsky and Bertrand, 2011). We study the spectral response of this profile to series of vertical SV plane waves of various angles of incidence, between -20° and 20° . Amplification has been calculated for both components of the velocity. The results obtained for the x-component of the velocity are very similar and nearly independent of the angle of incidence. The amplifications frequencies are in good accordance with real measurements data for two of the three stations we compared and seem to correspond to the fundamental frequency of the measurements data. The amplifications, calculated on the vertical velocity component, correspond to the higher frequencies of the real data. Numerical results of station 7 are not close to the real data. It may be due to the fact that this station, at the right side of the hill is close to the boundary. Note also that this study has been done using a 2D profile and could be extended to three dimensions of space.

REFERENCES

- Bertrand, E., Duval, A.-M., Régnier, J., Azzara, R.M., Bergamashi, F., Bordoni, P., Cara, F., Cultrera, G., Di Giulio, G., Milana, G. and Salichon, J. (2011). Site effect of the Roio basin, l'Aquila, *Bull. Earthq. Eng.*, **9:3**, 809-823.
- Delcourte, S., Fezoui, L. and Glinsky-Olivier, N. (2009). A high-order discontinuous method for the seismic wave equation, *ESAIM:Proceedings*, **27**, 70-89.
- De Martin, F. and Kobayashi, H. (2010). Etude des effets d'une topographie sur le mouvement sismique, Rapport BRGM/RP-59103-FR.
- Duval, A.-M. (2007). Des effets de site aux scénarios de crise sismique : méthodes et applications. Habilitation à diriger des recherches, Univ. Des Sciences et Technologies de Lille.
- Duval, A.-M., Bertrand, E., Régnier, J., Glinsky, N., Langlaude, P., Pernoud, M., Vidal, S., Gance, J., Grosso, E. and Semblat, J.-F. (2009). Experimental and numerical approaches of topographic site effect claimed to be responsible for 1909 Provence earthquake damage distribution, *American Geophysical Union*, Fall meeting, san Francisco.
- Gaffet, S. and Bouchon, M. (1989). Effects of two-dimensional topographies using the discrete wavenumber-boundary integral equation method in P-SV cases, *J. Acous. Soc. Am.*, **85**, 2277-2283.
- Glinsky, N. and Bertrand, E. (2011). Numerical study of topographical site effects by a discontinuous finite element method, *4th IASPEI/IAEE International Symposium "Effect of Surface Geology on Seismic Motion"*, Univ. California santa Barbara, August 23-26.
- Komatitsch, D. (1997). Méthodes spectrales et éléments spectraux pour l'équation de l'élastodynamique 2D et 3D en milieu hétérogène. Thèse de doctorat de l'Institut de Physique du Globe de Paris.